


RPiAE: A Representation-Pivoted Autoencoder Enhancing Both Image Generation and Editing

Yue Gong^{1,2*} Hongyu Li^{1*} Shanyuan Liu^{2*} Bo Cheng² Yuhang Ma² Liebucha Wu²
Xiaoyu Wu² Manyuan Zhang³ Dawei Leng^{2†} Yuhui Yin² Lijun Zhang^{1†}

¹Beihang University ²360 AI Research ³The Chinese University of Hong Kong
yuegong@buaa.edu.cn, lengdawei@360.cn, zhanglijun@buaa.edu.cn

Project Page: <https://arthuring.github.io/RPiAE-page/>

Abstract

Diffusion models have become the dominant paradigm for image generation and editing, with latent diffusion models shifting denoising to a compact latent space for efficiency and scalability. Recent attempts to leverage pretrained visual representation models as tokenizer priors either align diffusion features to representation features or directly reuse representation encoders as frozen tokenizers. Although such approaches can improve generation metrics, they often suffer from limited reconstruction fidelity due to frozen encoders, which in turn degrades editing quality, as well as overly high-dimensional latents that make diffusion modeling difficult. To address these limitations, We propose **Representation-Pivoted AutoEncoder**, a representation-based tokenizer that improves both generation and editing. We introduce Representation-Pivot Regularization, a training strategy that enables a representation-initialized encoder to be fine-tuned for reconstruction while preserving the semantic structure of the pretrained representation space, followed by a variational bridge which compress latent space into a compact one for better diffusion modeling. We adopt an objective-decoupled stage-wise training strategy that sequentially optimizes generative tractability and reconstruction-fidelity objectives. Together, these components yield a tokenizer that preserves strong semantics, reconstructs faithfully, and produces latents with reduced diffusion modeling complexity. Experiments demonstrate that RPiAE outperforms other visual tokenizers on text-to-image generation and image editing, while delivering the best reconstruction fidelity among representation-based tokenizers.

1 Introduction

Diffusion models have become the dominant paradigm for high-quality image generation and editing. Early diffusion systems operated in pixel space [15], but directly modeling high-resolution RGB images incurs heavy computation and memory costs and typically requires long denoising trajectories. As a result, latent diffusion models (LDM) [29] have become the mainstream choice by shifting the denoising process to a compact latent space, which is significantly more efficient and scalable.

Most recent progress has concentrated on improving the diffusion model itself—advancing architectures and training recipes from early LDM [29] to more powerful modern systems such as SD3 [10] and FLUX [19]. These efforts have led to rapid gains in generation quality and controllability.

*Equal contribution.

†Corresponding authors.

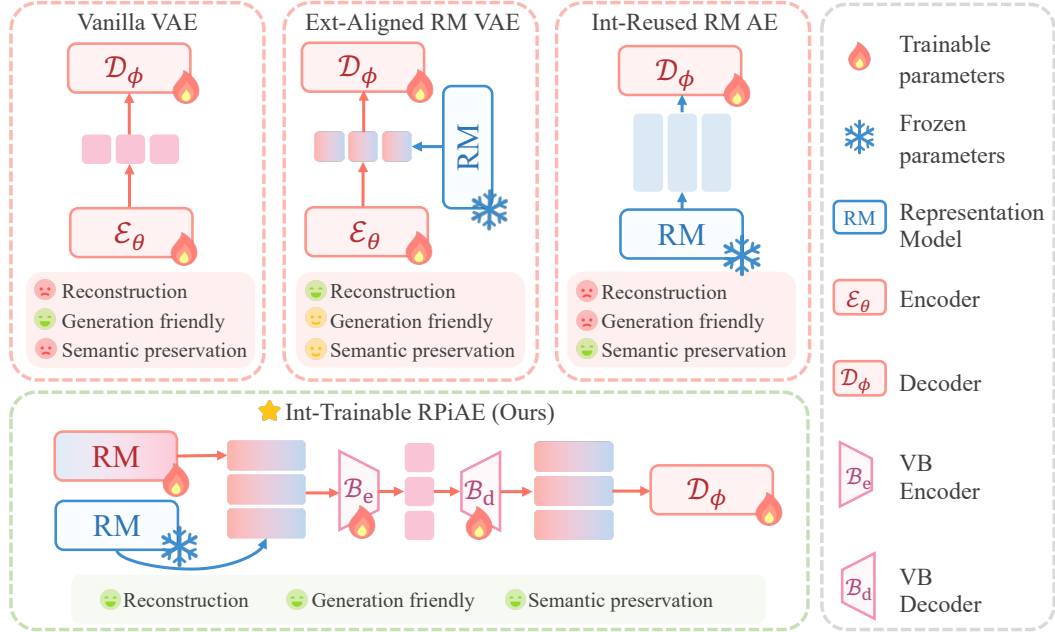


Figure 1: Motivation. A practical tokenizer for diffusion must simultaneously achieve high *reconstruction fidelity* for editing and strong *generative tractability* for diffusion training, while preserving the semantic structure of pretrained representation models.

However, this model-centric progress implicitly often inherits a legacy image tokenizer. The latent space and the tokenizer that defines it now form a critical bottleneck for downstream generation and editing, since latent diffusion performs denoising in the encoded latent space rather than directly in pixel space.

Because the diffusion model and the tokenizer share the same latent space, this space requires both *generative tractability* for denoising dynamics and *reconstruction fidelity* for high-fidelity decoding. From the denoising perspective, the diffusion model learns to remove noise directly in the latent space, so they are typically easier to train on latents that are more structured and semantically organized, with lower dimensionality and fewer high-frequency details. From the decoding perspective, the tokenizer must reconstruct images from latent representation. Richer latents with higher dimensionality and more high-frequency content naturally help recover fine details and preserve identity. These objectives are inherently in tension, making it challenging to strike the right balance between reconstruction and generation for optimal downstream performance.

In vanilla VAEs [29, 2], as illustrated in Fig. 1, the latent space is shaped mainly by the KL regularizer and thus often lacks a well-structured geometry, making downstream generative training difficult; as a result, the latent dimensionality is typically kept small, which in turn limits reconstruction fidelity.

Meanwhile, pretrained visual representation models (RMs) [25, 31, 28, 42] are primarily developed for image understanding, and thus produce features with rich semantics and a well-structured geometry. This structure provides a strong semantic prior with high *generative tractability*. A growing body of work has started to leverage such features to improve generative modeling. One representative direction, which we term *Ext-Aligned RM* methods, uses representation models as an external teacher to align and supervise diffusion training. These works [41, 39] align either diffusion-transformer intermediate features or autoencoder latent representations to pretrained RM features, injecting semantic structure to accelerate convergence and improve generation quality. However, the mismatch in dimensionality between RM features and generative latents makes such alignment inherently imperfect, preventing a full transfer of the representation geometry, suggesting further gains are still possible in generation quality.

More recent tokenization approaches [45, 30, 11], which we term *Int-Reused RM AE*, go one step further by directly reusing the representation model’s feature space for generation. They aim to fully

exploit its semantic structure and establish a shared latent space that supports both image generation and visual understanding by replacing the standard VAE encoder with a pretrained representation encoder and treat its feature space as the latent space for diffusion. While *Int-Reused RM AEs* can improve pure generation metrics, it faces two practical limitations. Freezing the representation encoder preserves semantic geometry but constrains reconstruction adaptation, reducing *reconstruction fidelity* and consequently hurting editing quality. Meanwhile, the high dimensionality of representation features reduces *generative tractability*, making diffusion modeling substantially harder and often requiring specialized designs. [45].

In this paper, We propose **Representation-Pivoted AutoEncoder (RPiAE)**, a tokenizer that jointly improves *reconstruction fidelity* and *generative tractability* by directly leveraging pretrained representation models. Our key observation is that unlocking a representation-initialized encoder can substantially raise the reconstruction ceiling, which is crucial for editing, but naïve reconstruction fine-tuning tends to corrupt the pretrained semantic geometry. RPiAE addresses this challenge by introduce Representation-Pivot Regularization training strategy. We regularize the trainable RME a with a frozen Pivot Replica Encoder and a Pivot Regularization loss, which keeps the trainable representation encoder anchored to the original representation space while it adapts for reconstruction, thereby preserving the semantic structure that benefits generation. To improve *generative tractability*, we further introduce a KL-regularized[14] Variational Bridge (VB) composed of an VB encoder and a VB decoder, which compresses the high-dimensional representation features into compact latents suited for diffusion modeling. To disentangle the competing objectives of improving *reconstruction fidelity*, enhancing *generative tractability*, and preserving the pretrained semantic geometry, we adopt an objective-decoupled, stage-wise training strategy that sequentially optimizes the three objectives—preserving representation semantics, improving reconstruction fidelity, and enhancing generative tractability.

In summary, our main contributions are as follows:

- We propose **RPiAE**, a representation-pivoted autoencoder that produces diffusion-friendly latents while preserving reconstruction fidelity for editing.
- We introduce **Representation-Pivot Regularization** and **Objective-Decoupled Training Strategy**, which enables a representation-initialized encoder to be fine-tuned for reconstruction while preserving the semantic structure of the representation space.
- Extensive experiments demonstrate that our method consistently outperforms existing image tokenizers on text-to-image generation, class-conditional generation, and image editing, while achieving the highest reconstruction fidelity among representation-based tokenizers.

2 Related Work

2.1 Visual Generation Models

Recent years have witnessed rapid progress in image generative modeling. Diffusion models have become one of the most successful paradigms for high-quality image synthesis, demonstrating strong capability in generating realistic and diverse images. Latent Diffusion Models (LDMs)[29, 10, 27] further improve computational efficiency by performing the denoising process in a compressed latent space learned by an autoencoder. Building on this paradigm, a series of works have explored more scalable and effective architectures for diffusion backbones, such as transformer-based models that enhance global context modeling and training scalability[26]. In parallel, alternative generative frameworks have also been investigated. In particular, flow-based generative[21, 24, 9] models have recently attracted renewed interest and shown promising results.

In parallel, downstream applications such as text-to-image generation [18, 38, 1, 36, 33] and instruction-based image editing [22, 35, 37] have advanced rapidly with the emergence of large-scale generative foundation models. These systems benefit from stronger text encoders, larger and cleaner training corpora, and improved alignment recipes, yielding substantial gains in prompt adherence, visual realism, and edit precision. More recently, unified multimodal models [6, 4] further integrate language and vision generation within a framework, strengthening text conditioning and enabling more controllable edits via richer instruction understanding, multi-turn interaction, and reasoning over multimodal context.

2.2 Generative Modeling with Representation Priors

A growing body of work leverages pretrained visual representation models as *representation priors* for diffusion-based generation[41, 20, 39, 44]. Existing approaches can be broadly categorized by how the representation model is used. One line of work treats the representation model as an external teacher and injects semantic structure through feature alignment. For example, REPA aligns intermediate states of diffusion transformers with features from pretrained visual encoders to improve convergence and generation quality[41]. Similar ideas have also been applied to tokenizer learning by aligning autoencoder latents with representation targets[39]. However, such alignment-based approaches often face *representation mismatch* between teacher and student features, requiring additional projection layers or heuristic design choices to bridge differences in dimensionality or tokenization. PS-VAE[44] instead adapts representation features for generation through a semantic-pixel reconstruction objective, jointly regularizing semantic representations and pixel reconstruction to learn compact generative latents. Concurrent to this line of work, our RPiAE takes a complementary route by directly reusing a representation-initialized tokenizer encoder and preserving its semantic geometry via Pivot Regularization during reconstruction fine-tuning, in a simple and direct manner, rather than transferring semantics through auxiliary reconstruction objectives.

Another line of work directly reuses pretrained representation encoders inside the tokenizer[45, 30, 11].RAE[45] replace the VAE encoder with a frozen representation encoder and train only the decoder, producing semantically latent spaces that benefit diffusion training[45]. FAE further introduces a feature encoder-decoder module to compress these high-dimensional features into lower-dimensional latents more suitable for generation[11]. Nevertheless, these approaches typically keep the representation encoder frozen, which limits reconstruction fidelity and is particularly detrimental for editing tasks where reconstruction errors accumulate. Our RPiAE bridges these paradigms by initializing the tokenizer encoder from a pretrained representation model while allowing it to be fine-tuned for reconstruction to reach strong reconstruction fidelity and effective generative modeling.

3 Method

We propose RPiAE, a representation-pivoted autoencoder designed to serve both image generation and editing. To support editing, it prioritizes high-fidelity reconstruction so as to preserve source identity and global consistency, which requires a trainable encoder that can adapt to the reconstruction objective. At the same time, to facilitate downstream latent diffusion training, RPiAE enforces a diffusion-friendly latent space by preserving the semantic structure of the pretrained representation while compressing it into a lower-dimensional bottleneck.

3.1 Overview of RPiAE

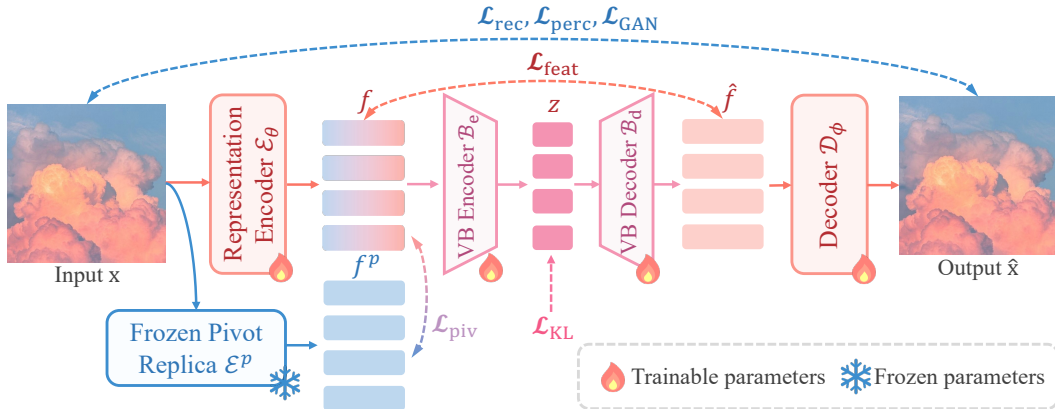


Figure 2: Overview of RPiAE. A pretrained RM encoder extracts representation features, which are compressed by a variational bridge into diffusion-friendly latents and decoded back for pixel-space reconstruction; a frozen pivot replica provides semantic supervision during training.

Fig.2 illustrates the overall architecture of RPiAE. Given an input image $\mathbf{x} \in \mathbb{R}^{C \times H \times W}$, RPiAE learns a representation-aware autoencoding pipeline with three trainable modules: a representation-model (RM) encoder \mathcal{E}_θ , a decoder \mathcal{D}_ϕ , and a Variational Bridge (VB). We build the RM encoder \mathcal{E}_θ directly on a pretrained representation model and initialize it with the pretrained weights, so that RPiAE can maximally inherit its high-quality semantic representations for generation. To seamlessly leverage the pretrained representation space, we instantiate \mathcal{E}_θ with the same architecture as the underlying representation model and initialize it from the pretrained weights. \mathcal{E}_θ encode the input image \mathbf{x} into a high dimensional representation feature $\mathbf{f} \in \mathbb{R}^{D \times h \times w}$, where $h = H/p$ and $w = W/p$ denote the spatial resolution after a patch size p . The VB is instantiated as an encoder-decoder pair $(\mathcal{B}_e, \mathcal{B}_d)$: \mathcal{B}_e compresses the high-dimensional, sparse features produced by \mathcal{E}_θ into a lower-dimensional, compact latent space denoted as $\mathbf{z} \in \mathbb{R}^{d \times h \times w}$, while \mathcal{B}_d maps \mathbf{z} back to the representational feature space. Finally, the decoder \mathcal{D}_ϕ transforms the decompressed features from VB back into the pixel space to reconstruct the image $\hat{\mathbf{x}} \in \mathbb{R}^{C \times H \times W}$. During reconstruction fine-tuning, \mathcal{E}_θ may drift away from its original semantic geometry; to mitigate this, we keep a frozen Pivot Replica Encoder(PRE) \mathcal{E}^p , which is architecturally identical and weight-initialized from the same pretrained model as \mathcal{E}_θ , as a fixed semantic reference that supervises the updates of \mathcal{E}_θ via the pivot feature $\mathbf{f}^p \in \mathbb{R}^{D \times h \times w}$ throughout training. The PRE is only used for training-time supervision and is discarded at inference, introducing no additional overhead during deployment.

To obtain generation-friendly latents, we regularize the VB latent space to be close to a standard normal distribution, since enforcing an approximately standard normal latent prior yields a smoother, well-conditioned latent space that better matches the assumptions of latent generative models and facilitates stable denoising-based training. Concretely, the VB encoder \mathcal{B}_e predicts the parameters of a diagonal Gaussian posterior from the representation feature \mathbf{f} and samples the latent code via the reparameterization method.

In All, The overall pipeline of RPiAE denotes as

$$\begin{aligned} \mathbf{f} &= \mathcal{E}_\theta(\mathbf{x}), & (\boldsymbol{\mu}, \log \boldsymbol{\sigma}^2) &= \mathcal{B}_e(\mathbf{f}), \\ \mathbf{z} &= \boldsymbol{\mu} + \boldsymbol{\sigma} \odot \boldsymbol{\epsilon}, & \boldsymbol{\epsilon} &\sim \mathcal{N}(\mathbf{0}, \mathbf{I}), \\ \hat{\mathbf{f}} &= \mathcal{B}_d(\mathbf{z}), & \hat{\mathbf{x}} &= \mathcal{D}_\phi(\hat{\mathbf{f}}). \end{aligned} \tag{1}$$

3.2 Unfreezing the RM Encoder with Pivot Regularization

Making the RM encoder trainable improves the reconstruction ceiling, but it may also cause the learned representation to drift away from the pretrained semantic geometry if optimized solely for pixel-level fidelity, as the model can become overly focused on high-frequency visual details. We therefore introduce **Pivot Regularization**, which regularizes the encoder feature \mathbf{f} to remain close to the pivot feature \mathbf{f}^p from frozen PRE \mathcal{E}^p while \mathcal{E}_θ is fine-tuned for reconstruction by pivot regularization loss \mathcal{L}_{piv} .

Since \mathcal{E}_θ is initialized from the same pretrained representation model as the frozen PRE \mathcal{E}^p , the features \mathbf{f} and \mathbf{f}^p start in the same representation space with compatible scale. We investigate two variants of pivot regularization loss: a raw ℓ_2 matching and a normalized- ℓ_2 matching. Table 1 compares their reconstruction and generation performance in terms of rFID and gFID. Overall, directly matching features with ℓ_2 yields better trade-offs. We attribute this to the fact that feature normalization discards informative magnitude cues and may distort the relative emphasis across tokens while the encoder is being fine-tuned for reconstruction. Moreover, the normalized- ℓ_2 objective can be overly permissive, allowing the encoder to drift more easily from the pretrained semantic geometry, which substantially degrades generation quality.

Table 1: \mathcal{L}_{piv} loss variants.

Loss	rFID↓	gFID↓
Norm- ℓ_2	0.16	9.85
ℓ_2	0.53	3.93

Table 2: Effect of adaptive weight for \mathcal{L}_{piv} .

λ_{piv}	rFID↓	gFID↓
w/o	0.68	7.56
w/	0.53	3.93

At the beginning of training, the encoder \mathcal{E}_θ and the pivot replica \mathcal{E}^p share the same initialization, making the discrepancy between \mathbf{f} and \mathbf{f}^p initially negligible, while the reconstruction loss can be

large. This imbalance may lead to unstable optimization. Inspired by GAN[13] loss and VA-VAE-style training, we employ an adaptive weight to balance \mathcal{L}_{piv} and the pixel-wise reconstruction loss \mathcal{L}_{rec} . As shown in Table 2, enabling adaptive weighting yields a more favorable reconstruction-generation trade-off than using a fixed weight.

In all, we define the pivot regularization loss \mathcal{L}_{piv} and its adaptive weight λ_{piv} as follows:

$$\begin{aligned}\mathcal{L}_{\text{rec}} &= \|\mathbf{x} - \hat{\mathbf{x}}\|_1, & \mathcal{L}_{\text{piv}} &= \lambda_{\text{piv}} \|\mathbf{f} - \mathbf{f}^p\|_2^2, \\ \mathbf{g}_{\text{rec}} &\triangleq \nabla_{\theta} \mathcal{L}_{\text{rec}}, & \mathbf{g}_{\text{piv}} &\triangleq \nabla_{\theta} \|\mathbf{f} - \mathbf{f}^p\|_2^2, \\ \lambda_{\text{piv}} &= \text{clip}\left(\frac{\|\mathbf{g}_{\text{rec}}\|}{\|\mathbf{g}_{\text{piv}}\| + \epsilon}, \lambda_{\text{min}}, \lambda_{\text{max}}\right).\end{aligned}\tag{2}$$

3.3 Objective-Decoupled Training Strategy

We adopt a three-stage training strategy as Fig. 3 to decouple objectives and improve stability. The key idea is to (I) obtain a reconstructable yet semantically stable encoder, (II) learn a compact KL-regularized latent via the Variational Bridge, and (III) specialize the decoder while keeping the latent structure fixed.

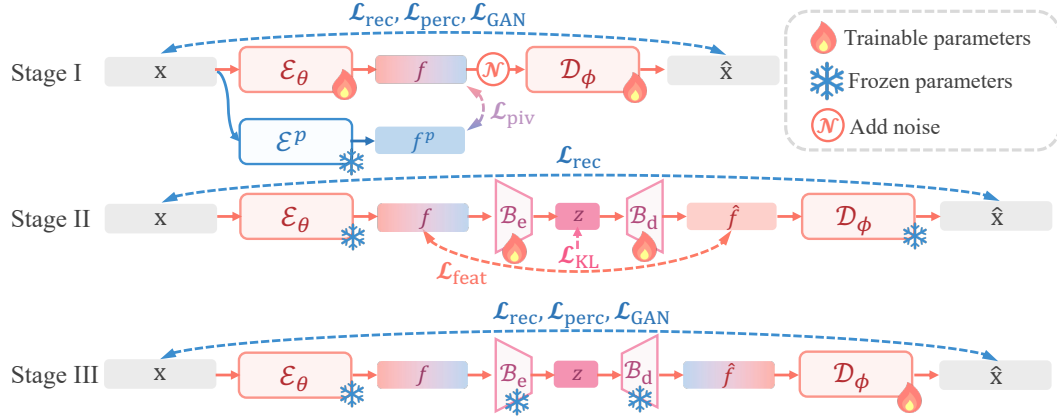


Figure 3: Three-stage training of RPiAE: (I) pivot-regularized encoder tuning, (II) variational bridge training with KL regularization, and (III) decoder specialization under fixed latents.

3.3.1 Stage I: Pivot-regularized encoder tuning.

We first train only E_θ and D_ϕ with reconstruction loss and pivoted regularization loss. This stage improves reconstruction while preventing representational drift through pivot regularization. Following LDM, we adopt a joint training objective that combines an adversarial (GAN) loss \mathcal{L}_{GAN} with a perceptual loss $\mathcal{L}_{\text{perc}}$. Following RAE to improve the decoder robustness, we inject Gaussian noise into the representation feature, which corresponds to decoding from the noise-smoothed distribution $p_{\mathbf{n}}(\mathbf{f}) = \int p(\mathbf{f} - \mathbf{n}) \mathcal{N}(\mathbf{n}; \mathbf{0}, \sigma^2 \mathbf{I}) d\mathbf{n}$, where $\mathbf{n} \sim \mathcal{N}(\mathbf{0}, \sigma^2 \mathbf{I})$. The over all loss of stage I is as follows:

$$\mathcal{L}_{\text{stageI}} = \mathcal{L}_{\text{rec}} + w_{\text{piv}} \mathcal{L}_{\text{piv}} + w_{\text{GAN}} \mathcal{L}_{\text{GAN}} + w_{\text{perc}} \mathcal{L}_{\text{perc}}.\tag{3}$$

3.3.2 Stage II: Variational Bridge training.

After Stage I, we freeze \mathcal{E}_θ and \mathcal{D}_ϕ and optimize only the Variational Bridge ($\mathcal{B}_e, \mathcal{B}_d$). We introduce a feature consistency loss $\mathcal{L}_{\text{feat}}$ between \mathbf{f} and $\hat{\mathbf{f}}$ to preserve the semantic structure of the representation while compressing it into the VB latent space. To prevent posterior collapse and regularize the latent distribution, we additionally impose a KL[14] term \mathcal{L}_{KL} on \mathbf{z} . For faster convergence, we also include a lightly weighted reconstruction loss \mathcal{L}_{rec} in this stage:

$$\begin{aligned}\mathcal{L}_{\text{stage2}} &= w_{\text{feat}} \mathcal{L}_{\text{feat}} + w_{\text{KL}} \mathcal{L}_{\text{KL}} + w_{\text{rec}} \mathcal{L}_{\text{rec}}, \\ \mathcal{L}_{\text{KL}} &= \text{KL}(q(\mathbf{z} | \mathbf{f}) \| \mathcal{N}(\mathbf{0}, \mathbf{I})).\end{aligned}\tag{4}$$

Table 3: Reconstruction and class-conditional generation on ImageNet-1K at 256². We report reconstruction metrics for the tokenizer and generation metrics for the diffusion model trained on the corresponding latents, evaluated both without and with CFG. † indicates reproducing results.

Method	Tokenizer	Image Reconstruction				#Params	Epochs	Generation w/o CFG				Generation w/ CFG			
		rFID↓	PSNR↑	LPIPS↓	SSIM↑			gFID↓	IS↑	Prec.↑	Rec.↑	gFID↓	IS↑	Prec.↑	Rec.↑
<i>Generation Models w/o RM</i>															
MaskGIT[3]	VQGAN[40]	2.23	17.9	0.202	0.422	227M	555	6.18	182.1	0.80	0.51	–	–	–	–
LlamaGen[32]	VQGAN[40]	0.59	24.5	–	0.813	3.1B	300	9.38	112.9	0.69	0.67	2.18	263.3	0.81	0.58
MaskDiT-XL[46]	SD-VAE[29]	0.61	26.9	0.130	0.736	675M	1600	5.69	177.9	0.74	0.60	2.28	276.6	0.80	0.61
DiT-XL[26]	SD-VAE[29]	0.61	26.9	0.130	0.736	675M	1400	9.62	121.5	0.67	0.67	2.27	278.2	0.83	0.57
SiT-XL[24]	SD-VAE[29]	0.61	26.9	0.130	0.736	675M	1400	8.61	131.7	0.68	0.67	2.06	270.3	0.82	0.59
<i>External-RM Aligned Generation Models</i>															
REPA-XL[41]	SD-VAE[29]	0.61	26.9	0.130	0.736	675M	80	7.90	–	–	–	–	–	–	–
SiT-XL[24]	VA-VAE[39]	0.27	27.7	0.097	0.779	675M	80	5.96	128.0	–	–	3.63	290.6	–	–
LightningDiT[39]	VA-VAE[39]	0.27	27.7	0.097	0.779	675M	64	5.14	130.2	0.76	0.62	–	–	–	–
<i>Internal-RM Generation Models</i>															
SVG-XL[30]	SVG[30]	0.65	–	–	–	675M	80	6.57	137.9	–	–	3.54	207.6	–	–
LightningDiT†[39]	RAE-S[45]	0.64	18.9	0.252	0.489	675M	80	3.05	166.1	0.79	0.60	–	–	–	–
LightningDiT†[39]	RAE-B[45]	0.57	18.8	0.256	0.483	675M	80	3.33	189.9	0.82	0.55	–	–	–	–
DiT ^{RM} -XL[45]	RAE-B[45]	0.57	18.8	0.256	0.483	839M	80	2.16	214.8	0.82	0.59	1.74	235.0	0.81	0.60
LightningDiT[39]	FAE-d32[11]	0.68	–	–	–	675M	80	2.08	207.6	0.82	0.59	1.70	243.8	0.82	0.61
LightningDiT[39]	RPiAE (Ours)	0.50	21.3	0.216	0.525	675M	60	2.46	201.1	0.80	0.59	2.06	208.5	0.80	0.61
LightningDiT[39]	RPiAE (Ours)	0.50	21.3	0.216	0.525	675M	80	2.25	208.7	0.81	0.60	1.51	225.9	0.79	0.65

where $\mathcal{L}_{\text{feat}}$ measures the discrepancy between $\hat{\mathbf{f}} = \mathcal{B}_d(\mathbf{z})$ and \mathbf{f} (we use an ℓ_2 loss in our implementation). This stage learns a compact latent space with a simple prior while retaining informative semantics for downstream generative modeling.

3.3.3 Stage III: Decoder specialization.

Finally, we freeze \mathcal{E}_θ and the Variational Bridge ($\mathcal{B}_e, \mathcal{B}_d$), and fine-tune the decoder \mathcal{D}_ϕ to maximize reconstruction quality under the fixed latent structure:

$$\mathcal{L}_{\text{stageIII}} = \mathcal{L}_{\text{rec}} + w_{\text{GAN}} \mathcal{L}_{\text{GAN}} + w_{\text{perc}} \mathcal{L}_{\text{perc}}. \quad (5)$$

This stage improves perceptual fidelity and mitigates reconstruction-induced artifacts that can otherwise degrade editing quality.

4 Experiments

To evaluate the effectiveness of RPiAE for both generation and editing, we conduct experiments on image reconstruction, class-conditional image generation, text-to-image synthesis, and image editing.

4.1 Experimental Setting

For the RM encoder, we adopt DINOv2-B [25] as \mathcal{E}_θ , producing representation features with channel dimension $D = 768$. The Variational Bridge ($\mathcal{B}_e, \mathcal{B}_d$) is implemented as a multi-layer Transformer[34], where \mathcal{B}_e uses 1 encoder layer and \mathcal{B}_d uses 6 decoder layers. We set the latent dimension of \mathbf{z} to $d = 64$ and use a patch size of $p = 16$. For the pixel decoder, we use a ViT-XL[7] backbone as \mathcal{D}_ϕ . The discriminator used for GAN is a ViT-S[7] initialized from DINOv2-S[25].

4.2 Image Reconstruction and Class-conditional Image Generation

4.2.1 Implementation details

In image reconstruction training, we use ImageNet-1K[5] at 256×256 resolution. Stage I is trained for 16 epochs with noise level $\sigma = 0.8$. Unless otherwise specified, we set $w_{\text{div}} = 1$ and $w_{\text{perc}} = 1$; for adversarial learning, we compute the GAN[13] loss weight using an adaptive weighting scheme and set $w_{\text{GAN}} = 0.75$. Stage II is trained for 32 epochs with $w_{\text{KL}} = 0.001$ and a lightly weighted reconstruction term $w_{\text{rec}} = 0.05$. Stage III is trained for 16 epochs, using the same loss weights as Stage I. Global batch size is set to 512. We apply a cosine learning-rate schedule with a 1-epoch warmup from zero, decaying until epoch 16 from a base learning rate of 2×10^{-4} to a final learning rate of 2×10^{-5} . We evaluate class-conditional image generation on ImageNet-1K[5] using LightningDiT as the downstream diffusion transformer. The generator operates on latent inputs of size 16×16 with 64 channels. Our LightningDiT architecture and hyperparameter settings follow those of VA-VAE[39].

Table 4: Comparison of different Method for Text-to-Image Generation and Image Editing on GenEval, DPG-Bench and GEdit-Bench-EN.

Method	GenEval							DPG-Bench	GEdit-Bench-EN		
	Sin.Obj.	Two.Obj.	Counting	Colors	Pos	Color.Attr.	Overall	Average	G_SC	G_PQ	G_O
<i>Open-source Models</i>											
Flux-VAE [18]	0.93	0.68	0.48	0.76	0.51	0.44	0.63	77.44	3.71	8.42	3.86
RAE-DINOv2-S[45]	0.97	0.78	0.52	0.81	0.60	0.52	0.70	80.81	2.86	7.04	3.09
RAE-DINOv2-B [45]	0.93	0.65	0.46	0.73	0.47	0.37	0.60	78.58	2.71	8.03	3.12
+ DDT Head	0.96	0.81	0.51	0.82	0.59	0.44	0.69	80.82	3.25	7.76	3.51
VAVAE [39]	0.96	0.73	0.44	0.83	0.49	0.53	0.66	78.69	2.09	7.69	2.26
+ DDT Head	0.94	0.74	0.38	0.83	0.47	0.53	0.65	80.32	2.04	7.89	2.27
<i>Ours</i>											
RPiAE	0.96	0.86	0.64	0.82	0.63	0.58	0.75	82.59	5.23	8.34	5.25
+ DDT Head	0.97	0.86	0.62	0.89	0.66	0.56	0.76	83.34	5.05	7.86	5.09

We train the model for 80 epochs with a global batch size of 1024, EMA decay 0.9995. Optimization is performed using AdamW with learning rate 2×10^{-4} , $(\beta_1, \beta_2) = (0.9, 0.95)$. For guidance, we follow RAE[45] and adopt AutoGuidance in place of standard classifier-free guidance.

4.2.2 Evaluation and Result on Image Reconstruction

We evaluate the image reconstruction capability of tokenizers on ImageNet-1K[5] validation set using reconstruction FID (rFID), PSNR, LPIPS[43], and SSIM, which respectively measure distribution-level reconstruction quality, pixel-level fidelity, perceptual similarity, and structural consistency. To assess class-conditional generation performance, we sample 50K images by the equal class sample strategy follow RAE to evaluate the matrix of generation. We report generation FID (gFID), Inception Score (IS), Precision, and Recall, which together reflect generation quality, spatial fidelity, sample diversity, and the trade-off between fidelity and coverage.

The results are summarized in Table 3. Among all Internal-RM tokenizers, our model achieves the best rFID, second only to VA-VAE. These results verify that enabling reconstruction-oriented fine-tuning of the RM encoder substantially improves the reconstruction capacity of Internal-RM tokenizers. Importantly, the gain in reconstruction does not come at the expense of generation. Instead, our tokenizer also achieves state-of-the-art generation performance. At 80 epochs, it reaches a gFID of 2.25 without CFG and 1.51 with CFG, establishing a new best result.

Overall, the results show that, under our representation-pivoted training strategy and architectural design, RPiAE improves reconstruction while preserving the semantic structure of the encoder. At the same time, it effectively compresses semantically rich high-dimensional representation features into a generation-friendly low-dimensional latent space, thereby improving both reconstruction and generation performance simultaneously.

4.3 Text-to-Image Generation and Image Edit

4.3.1 Implementation details

To ensure fair comparison, we establish a unified evaluation protocol for evaluating the text-to-image generation and image editing capabilities of different visual tokenizers. We build our image-generation model on the Bagel-MoT [6] architecture, initialized from Qwen25-0.5B [38]. All images are resized to 256×256 , and we train on CC12M-LLaVA-Next [8] for 200K iterations, with 384K–400K tokens per iteration. Building on the text-to-image generation model, we further fine-tune it for image editing on the OmniEdit [35] dataset for 50K iterations, using 192K–200K tokens per iteration. We compute the time shift following the formulation in RAE [45]. During inference, we use classifier-free guidance (CFG) with 4.

4.3.2 Evaluation and Results on Text-to-Image Generation and Image Editing

We evaluate text-to-image generation using GenEval [12] (with the Bagel rewritten prompts [6]) and DPG-Bench [16], and assess image editing on GEdit-Bench-EN [22]. For efficiency and reproducibility, we adopt EditScore-Qwen3VL-8B [23] to compute VieScore [17], which includes three dimensions: G_SC , G_PQ , and G_O . Here, G_SC measures instruction following, G_PQ evaluates generation quality and identity/preservation, and G_O aggregates the overall performance.

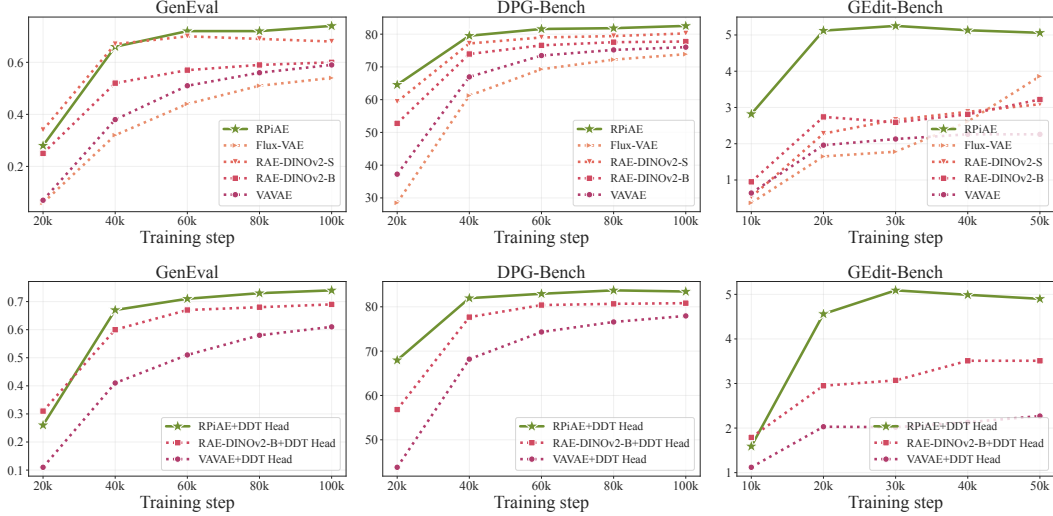


Figure 4: Performance of GenEval, DPG-Bench, and GEdit over training for different encoders. Our method achieves both a higher performance ceiling and faster convergence.

As shown in table 4, our method achieves the best results across all benchmarks, both with and without the DDT head; moreover, adding the DDT head further improves T2I generation quality. The training curves in fig. 4 also demonstrate that our approach converges faster and exhibits more stable optimization, with particularly pronounced gains in image editing.

4.4 Qualitative Results

We provide qualitative visualizations in fig. 5 to complement the quantitative results. RPiAE follows prompts and editing instructions more faithfully, producing sharper details and more coherent structures while better preserving source identity. In contrast, other tokenizers more often suffer from over-smoothing, semantic drift, and background leakage.

4.5 Ablation Study

4.5.1 Ablation on Objective-Decoupled Training Strategy

We evaluate RPiAE at different training stages on reconstruction, text-to-image generation, and image editing. As shown in Table 5a, Stage I achieves strong reconstruction but suffers in generation/editing due to uncompressed high-dimensional latents. Stage II introduces the VB to learn compact diffusion-friendly latents, substantially improving generation, while freezing the decoder limits reconstruction and editing fidelity. Stage III fine-tunes the decoder under a fixed latent space, recovering reconstruction quality and boosting editing. A single-stage joint training baseline performs worse overall, supporting our objective-decoupled stage-wise strategy.

4.5.2 Ablation on Training the Encoder and the decoder structure

To verify the effectiveness of our Pivot Regularization for RM encoder training, we conduct an ablation study on whether the encoder is unfrozen and trained with Pivot Regularization in Stage I. To demonstrate that our conclusion is not tied to a specific decoder design, we further evaluate different decoder architectures. In particular, we replace our default decoder with the SD-VAE decoder and repeat the experiments.

The results in Table 5b show that, regardless of whether the decoder is CNN-based or ViT-based, unfreezing the encoder and applying Pivot Regularization consistently improves reconstruction performance. Specifically, the rFID improves from 1.35 to 0.65 with the SD-style decoder and from 0.62 to 0.50 with the ViT decoder. The improved reconstruction quality also translates into better visual fidelity in image editing, while maintaining nearly unchanged text-to-image generation performance, as reflected by similar GenEval scores.

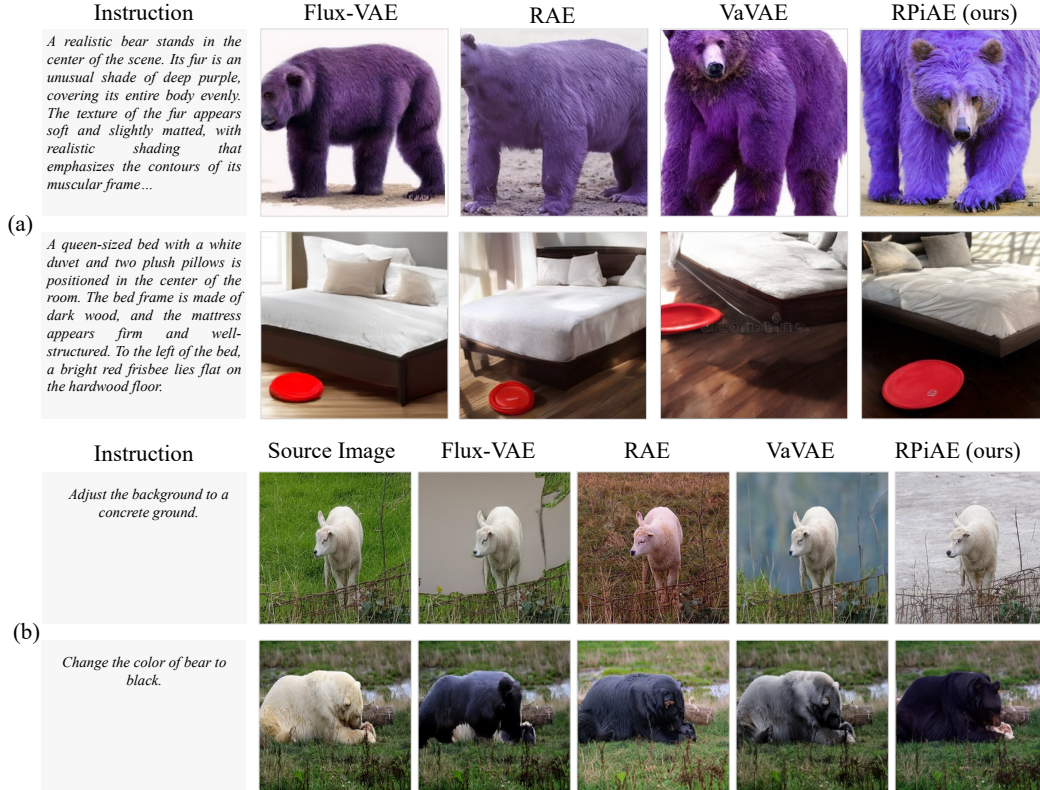


Figure 5: Visualizations of Text to Image Generation in (a) and Image Editing in (b).

4.5.3 Ablation on Latent Space Dimension

To study the effect of the latent dimensionality on reconstruction, generation, and editing, we perform an ablation over the latent space dimension d . As shown in Table 5c, increasing d consistently improves reconstruction quality, indicating that a higher-dimensional latent space preserves more information for faithful image recovery. However, overly large latent dimensions lead to worse performance in both image generation and image editing. This trade-off suggests that, while a larger latent space benefits reconstruction, it also makes the latent distribution less favorable for downstream generative modeling. In practice, we therefore choose $d = 64$ as a balanced setting, which achieves a strong compromise between reconstruction fidelity and generation/editing performance, and use it for all main results.

4.5.4 Ablation on Pivot Regularization Loss Weight

To study the effect of the pivot-regularization weight, we ablate w_{piv} , with results reported in Table 2. As w_{piv} decreases, the supervision strength of Pivot Regularization on the RM encoder becomes weaker and the optimization increasingly favors reconstruction. Consequently, the reconstruction rFID improves and the editing quality score G_{PQ} also increases. However, the weaker constraint reduces how well the encoder preserves the semantic structure of the pretrained representation model, leading to degraded generation quality and lower editing success rates. We therefore adopt $w_{\text{piv}} = 1$ in our final setting, which provides the best overall trade-off.

5 Conclusion

We presented RPiAE, a representation-pivoted autoencoder that improves both reconstruction fidelity and generative tractability for diffusion models. Our key idea is to fine-tune a representation-initialized encoder for reconstruction while preventing semantic drift via Pivot Regularization, and to compress high-dimensional representation features into compact diffusion-friendly latents with a

Table 5: Ablation studies on GEdit-Bench-EN / ImgEdit-Bench.

(a) Objective-decoupled training strategy							(b) Decoder type and Trainable encoder.					
S.I	S.II	S.III	rFID↓	GenEval↑	GEdit-Bench-EN ↑		Dec	T. \mathcal{E}_θ	rFID↓	GenEval↑	GEdit-Bench-EN ↑	
					G_SC	G_PQ					G_SC	G_PQ
✓	✗	✗	0.47	0.58	2.79	8.33	SD-dec.	✗	1.35	0.71	4.68	7.68
✓	✓	✗	1.57	0.74	4.72	7.87	SD-dec.	✓	0.65	0.71	4.49	8.01
✓	✓	✓	0.50	0.75	5.23	8.34	ViT-XL	✗	0.62	0.76	5.04	8.03
Single Stage			0.64	0.73	4.84	8.16	ViT-XL	✓	0.50	0.75	5.23	8.34

(c) Dimension of latent ablation.					(d) Weight of \mathcal{L}_{piv} ablation.				
d	rFID↓	GenEval↑	GEdit-Bench-EN ↑		w_{piv}	rFID↓	GenEval↑	GEdit-Bench-EN ↑	
			G_SC	G_PQ				G_SC	G_PQ
32	0.58	0.73	5.34	8.01	1	0.50	0.75	5.23	8.34
64	0.50	0.75	5.23	8.34	0.5	0.33	0.69	5.04	8.49
128	0.47	0.70	5.15	8.28	0.25	0.22	0.65	4.66	8.77

KL-regularized Variational Bridge. Experiments show that RPiAE achieves strong reconstruction while delivering state-of-the-art generation and editing performance among representation-based tokenizers.

References

- [1] Bai, S., Chen, K., Liu, X., Wang, J., Ge, W., Song, S., Dang, K., Wang, P., Wang, S., Tang, J., Zhong, H., Zhu, Y., Yang, M., Li, Z., Wan, J., Wang, P., Ding, W., Fu, Z., Xu, Y., Ye, J., Zhang, X., Xie, T., Cheng, Z., Zhang, H., Yang, Z., Xu, H., Lin, J.: Qwen2.5-vl technical report (2025), <https://arxiv.org/abs/2502.13923>
- [2] Cemgil, T., Ghaisas, S., Dvijotham, K., Gowal, S., Kohli, P.: The autoencoding variational autoencoder. *Advances in Neural Information Processing Systems* **33**, 15077–15087 (2020)
- [3] Chang, H., Zhang, H., Jiang, L., Liu, C., Freeman, W.T.: Maskgit: Masked generative image transformer. In: *Proceedings of the IEEE/CVF conference on computer vision and pattern recognition*. pp. 11315–11325 (2022)
- [4] Cui, Y., Chen, H., Deng, H., Huang, X., Li, X., Liu, J., Liu, Y., Luo, Z., Wang, J., Wang, W., et al.: Emu3. 5: Native multimodal models are world learners. *arXiv preprint arXiv:2510.26583* (2025)
- [5] Deng, B., Heath, L.: Toward errorless training imagenet-1k (2025), <https://arxiv.org/abs/2508.04941>
- [6] Deng, C., Zhu, D., Li, K., Gou, C., Li, F., Wang, Z., Zhong, S., Yu, W., Nie, X., Song, Z., et al.: Emerging properties in unified multimodal pretraining. *arXiv preprint arXiv:2505.14683* (2025)
- [7] Dosovitskiy, A., Beyer, L., Kolesnikov, A., Weissenborn, D., Zhai, X., Unterthiner, T., Dehghani, M., Minderer, M., Heigold, G., Gelly, S., Uszkoreit, J., Houlsby, N.: An image is worth 16x16 words: Transformers for image recognition at scale (2021), <https://arxiv.org/abs/2010.11929>
- [8] Emporium, C.: conceptual-captions-cc12m-llavanext. <https://huggingface.co/datasets/CaptionEmporium/conceptual-captions-cc12m-llavanext> (2024)
- [9] Esser, P., Kulal, S., Blattmann, A., Entezari, R., Müller, J., Saini, H., Levi, Y., Lorenz, D., Sauer, A., Boesel, F., et al.: Scaling rectified flow transformers for high-resolution image synthesis. In: *Forty-first international conference on machine learning* (2024)

- [10] Esser, P., Kulal, S., Blattmann, A., Entezari, R., Müller, J., Saini, H., Levi, Y., Lorenz, D., Sauer, A., Boesel, F., Podell, D., Dockhorn, T., English, Z., Lacey, K., Goodwin, A., Marek, Y., Rombach, R.: Scaling rectified flow transformers for high-resolution image synthesis (2024), <https://arxiv.org/abs/2403.03206>
- [11] Gao, Y., Chen, C., Chen, T., Gu, J.: One layer is enough: Adapting pretrained visual encoders for image generation. arXiv preprint arXiv:2512.07829 (2025)
- [12] Ghosh, D., Hajishirzi, H., Schmidt, L.: Geneval: An object-focused framework for evaluating text-to-image alignment. *Advances in Neural Information Processing Systems* **36**, 52132–52152 (2023)
- [13] Goodfellow, I.J., Pouget-Abadie, J., Mirza, M., Xu, B., Warde-Farley, D., Ozair, S., Courville, A., Bengio, Y.: Generative adversarial networks (2014), <https://arxiv.org/abs/1406.2661>
- [14] GX-Chen, A., Prakash, J., Guo, J., Fergus, R., Ranganath, R.: Kl-regularized reinforcement learning is designed to mode collapse (2025), <https://arxiv.org/abs/2510.20817>
- [15] Ho, J., Jain, A., Abbeel, P.: Denoising diffusion probabilistic models. *Advances in neural information processing systems* **33**, 6840–6851 (2020)
- [16] Hu, X., Wang, R., Fang, Y., Fu, B., Cheng, P., Yu, G.: Ella: Equip diffusion models with llm for enhanced semantic alignment. arXiv preprint arXiv:2403.05135 (2024)
- [17] Ku, M., Jiang, D., Wei, C., Yue, X., Chen, W.: Viescore: Towards explainable metrics for conditional image synthesis evaluation. In: *Proceedings of the 62nd Annual Meeting of the Association for Computational Linguistics (Volume 1: Long Papers)*. pp. 12268–12290 (2024)
- [18] Labs, B.F.: Flux. <https://github.com/black-forest-labs/flux> (2024)
- [19] Labs, B.F., Batifol, S., Blattmann, A., Boesel, F., Consul, S., Diagne, C., Dockhorn, T., English, J., English, Z., Esser, P., et al.: Flux. 1 kontext: Flow matching for in-context image generation and editing in latent space. arXiv preprint arXiv:2506.15742 (2025)
- [20] Leng, X., Singh, J., Hou, Y., Xing, Z., Xie, S., Zheng, L.: Repa-e: Unlocking vae for end-to-end tuning of latent diffusion transformers. In: *Proceedings of the IEEE/CVF International Conference on Computer Vision*. pp. 18262–18272 (2025)
- [21] Lipman, Y., Chen, R.T.Q., Ben-Hamu, H., Nickel, M., Le, M.: Flow matching for generative modeling. In: *The Eleventh International Conference on Learning Representations* (2023), <https://openreview.net/forum?id=PqvMRDCJT9t>
- [22] Liu, S., Han, Y., Xing, P., Yin, F., Wang, R., Cheng, W., Liao, J., Wang, Y., Fu, H., Han, C., et al.: Step1x-edit: A practical framework for general image editing. arXiv preprint arXiv:2504.17761 (2025)
- [23] Luo, X., Wang, J., Wu, C., Xiao, S., Jiang, X., Lian, D., Zhang, J., Liu, D., et al.: Editscore: Unlocking online rl for image editing via high-fidelity reward modeling. arXiv preprint arXiv:2509.23909 (2025)
- [24] Ma, N., Goldstein, M., Albergo, M.S., Boffi, N.M., Vanden-Eijnden, E., Xie, S.: Sit: Exploring flow and diffusion-based generative models with scalable interpolant transformers. In: *European Conference on Computer Vision*. pp. 23–40. Springer (2024)
- [25] Oquab, M., Darcet, T., Moutakanni, T., Vo, H., Szafraniec, M., Khalidov, V., Fernandez, P., Haziza, D., Massa, F., El-Nouby, A., Assran, M., Ballas, N., Galuba, W., Howes, R., Huang, P.Y., Li, S.W., Misra, I., Rabbat, M., Sharma, V., Synnaeve, G., Xu, H., Jegou, H., Mairal, J., Labatut, P., Joulin, A., Bojanowski, P.: Dinov2: Learning robust visual features without supervision (2024), <https://arxiv.org/abs/2304.07193>
- [26] Peebles, W., Xie, S.: Scalable diffusion models with transformers. In: *Proceedings of the IEEE/CVF International Conference on Computer Vision*. pp. 4195–4205 (2023)

- [27] Podell, D., English, Z., Lacey, K., Blattmann, A., Dockhorn, T., Müller, J., Penna, J., Rombach, R.: Sdxl: Improving latent diffusion models for high-resolution image synthesis (2023), <https://arxiv.org/abs/2307.01952>
- [28] Radford, A., Kim, J.W., Hallacy, C., Ramesh, A., Goh, G., Agarwal, S., Sastry, G., Askell, A., Mishkin, P., Clark, J., et al.: Learning transferable visual models from natural language supervision. In: International conference on machine learning. pp. 8748–8763. PmLR (2021)
- [29] Rombach, R., Blattmann, A., Lorenz, D., Esser, P., Ommer, B.: High-resolution image synthesis with latent diffusion models. In: Proceedings of the IEEE/CVF conference on computer vision and pattern recognition. pp. 10684–10695 (2022)
- [30] Shi, M., Wang, H., Zheng, W., Yuan, Z., Wu, X., Wang, X., Wan, P., Zhou, J., Lu, J.: Latent diffusion model without variational autoencoder (2026), <https://arxiv.org/abs/2510.15301>
- [31] Siméoni, O., Vo, H.V., Seitzer, M., Baldassarre, F., Oquab, M., Jose, C., Khalidov, V., Szafraniec, M., Yi, S., Ramamonjisoa, M., Massa, F., Haziza, D., Wehrstedt, L., Wang, J., Darcet, T., Moutakanni, T., Sentana, L., Roberts, C., Vedaldi, A., Tolan, J., Brandt, J., Couprie, C., Mairal, J., Jégou, H., Labatut, P., Bojanowski, P.: Dinov3 (2025), <https://arxiv.org/abs/2508.10104>
- [32] Sun, P., Jiang, Y., Chen, S., Zhang, S., Peng, B., Luo, P., Yuan, Z.: Autoregressive model beats diffusion: Llama for scalable image generation (2024), <https://arxiv.org/abs/2406.06525>
- [33] Team, M.L., Ma, H., Tan, H., Huang, J., Wu, J., He, J.Y., Gao, L., Xiao, S., Wei, X., Ma, X., et al.: Longcat-image technical report. arXiv preprint arXiv:2512.07584 (2025)
- [34] Vaswani, A., Shazeer, N., Parmar, N., Uszkoreit, J., Jones, L., Gomez, A.N., Kaiser, L., Polosukhin, I.: Attention is all you need (2023), <https://arxiv.org/abs/1706.03762>
- [35] Wei, C., Xiong, Z., Ren, W., Du, X., Zhang, G., Chen, W.: Omniedit: Building image editing generalist models through specialist supervision. In: The Thirteenth International Conference on Learning Representations (2024)
- [36] Wu, C., Li, J., Zhou, J., Lin, J., Gao, K., Yan, K., Yin, S.m., Bai, S., Xu, X., Chen, Y., et al.: Qwen-image technical report. arXiv preprint arXiv:2508.02324 (2025)
- [37] Wu, C., Zheng, P., Yan, R., Xiao, S., Luo, X., Wang, Y., Li, W., Jiang, X., Liu, Y., Zhou, J., et al.: Omnigen2: Exploration to advanced multimodal generation. arXiv preprint arXiv:2506.18871 (2025)
- [38] Yang, A., Li, A., Yang, B., Zhang, B., Hui, B., Zheng, B., Yu, B., Gao, C., Huang, C., Lv, C., et al.: Qwen3 technical report. arXiv preprint arXiv:2505.09388 (2025)
- [39] Yao, J., Yang, B., Wang, X.: Reconstruction vs. generation: Taming optimization dilemma in latent diffusion models. In: Proceedings of the Computer Vision and Pattern Recognition Conference. pp. 15703–15712 (2025)
- [40] Yu, J., Li, X., Koh, J.Y., Zhang, H., Pang, R., Qin, J., Ku, A., Xu, Y., Baldrige, J., Wu, Y.: Vector-quantized image modeling with improved vqgan (2022), <https://arxiv.org/abs/2110.04627>
- [41] Yu, S., Kwak, S., Jang, H., Jeong, J., Huang, J., Shin, J., Xie, S.: Representation alignment for generation: Training diffusion transformers is easier than you think. arXiv preprint arXiv:2410.06940 (2024)
- [42] Zhai, X., Mustafa, B., Kolesnikov, A., Beyer, L.: Sigmoid loss for language image pre-training (2023), <https://arxiv.org/abs/2303.15343>
- [43] Zhang, R., Isola, P., Efros, A.A., Shechtman, E., Wang, O.: The unreasonable effectiveness of deep features as a perceptual metric. In: Proceedings of the IEEE conference on computer vision and pattern recognition. pp. 586–595 (2018)

- [44] Zhang, S., Zhang, H., Zhang, Z., Ge, C., Xue, S., Liu, S., Ren, M., Kim, S.Y., Zhou, Y., Liu, Q., et al.: Both semantics and reconstruction matter: Making representation encoders ready for text-to-image generation and editing. arXiv preprint arXiv:2512.17909 (2025)
- [45] Zheng, B., Ma, N., Tong, S., Xie, S.: Diffusion transformers with representation autoencoders. In: The Fourteenth International Conference on Learning Representations (2026), <https://openreview.net/forum?id=0u1LigJaab>
- [46] Zheng, H., Nie, W., Vahdat, A., Anandkumar, A.: Fast training of diffusion models with masked transformers (2024), <https://arxiv.org/abs/2306.09305>

A More Implementation Details

This section provides additional implementation details for both the main and preliminary experiments, including the training configurations of RPiAE and the corresponding generator settings.

A.1 More Implementation Details of RPiAE in Main Experiments

Table 6 provides the implementation details of the RPiAE tokenizer and the LightningDiT generator used in our main experiments. The RPiAE configuration listed here is the one adopted for all primary results in the main paper, including those reported in Table 3, Table 4, and Fig. 4 in main paper.

Table 6: Implementation details of RPiAE and LightningDiT used in our experiments.

Category	Field	\mathcal{E}_θ	\mathcal{D}_ϕ	\mathcal{E}^p	\mathcal{B}_e	\mathcal{B}_d	LightningDiT
Architecture	Input dim.	$224 \times 224 \times 3$	$16 \times 16 \times 768$	$224 \times 224 \times 3$	$16 \times 16 \times 768$	$16 \times 16 \times 64$	$16 \times 16 \times 64$
	Output dim.	$16 \times 16 \times 768$	$256 \times 256 \times 3$	$16 \times 16 \times 768$	$16 \times 16 \times 64$	$16 \times 16 \times 768$	$16 \times 16 \times 64$
	Hidden dim.	768	1536	768	768	768	1152
	Num. layers	12	24	12	1	6	28
	MLP Ratio	4	4	4	1	4	4
	Dim. per head	64	64	64	96	96	72
	Num. heads	12	24	12	8	8	16
	Total Params (M)	86.58M	415.35M	86.58M	4.24M	43.17M	675.63M
Optimization	Training iters	4×10^4 (Stage I)	4×10^4 (Stage I)	–	–	–	–
	Batch size	–	–	–	8×10^4 (Stage II)	8×10^4 (Stage II)	10^5
	Optimizer	AdamW	AdamW	–	AdamW	AdamW	AdamW
	Peak LR	2×10^{-4}	2×10^{-4}	–	2×10^{-4}	2×10^{-4}	2×10^{-4}
	LR Scheduler	Cosine	Cosine	–	Cosine	Cosine	Linear
	Warmup	1 epoch	1 epoch	–	1 epoch	1 epoch	40 epochs
	(β_1, β_2)	(0.9, 0.95)	(0.9, 0.95)	–	(0.9, 0.95)	(0.9, 0.95)	(0.9, 0.95)
	Interpolants	α_t	–	–	–	–	–
	σ_t	–	–	–	–	–	t
	Training objective	reconstruction	reconstruction	–	reconstruction	reconstruction	v-prediction
	Sampler	–	–	–	–	–	Euler (ODE)
	Sampling steps	–	–	–	–	–	50
	Guidance	–	–	–	–	–	2.05 (auto-guidance, $t = 0 \sim 1$)

A.2 Implementation Details of RPiAE for Preliminary Experiments

Table 7 summarizes the implementation details of the preliminary experiments used to select the Pivot Regularization strategy introduced in Section 3.2. The configurations reported here are those used for the preliminary results in Table 1 and Table 2 of the main paper. Compared with the main experiments, we adopt a lighter CNN-based decoder, similar to the SD [29] decoder, to accelerate experimental iteration. In addition, we only conduct Stage I training for the tokenizer, and then combine the trained tokenizer with DiT^{DH} to obtain a fast validation of its generative capability, using the same diffusion-model configuration as in RAE [45].

B More Quantitative Results

Table 8 further extends the class-conditional image generation results in the main paper. While Table 3 in the main paper shows that RPiAE already achieves strong performance at an early training stage, demonstrating fast convergence in class-conditional generation, here we further prolong the training from the main setting to 800 epochs, corresponding to 10^6 training iterations, in order to examine the upper-bound generation performance of RPiAE under a longer optimization budget. For evaluation, we adopt 250 sampling steps together with auto-guidance.

The results show that RPiAE delivers the strongest overall performance among internal-RM models under this extended training setting. Without CFG, RPiAE achieves the best Inception Score of 254.7, indicating superior sample quality and class-consistency. With CFG, RPiAE obtains the best gFID of 1.09 and the best Rec. of 0.70, suggesting that it not only produces high-fidelity samples but also maintains stronger sample diversity. These results further confirm that the latent space learned by RPiAE is highly effective for class-conditional diffusion modeling, and that its advantage persists when the generation model is trained to a more fully converged regime.

Table 7: Implementation details of RPiAE and DiT^{DH} used in our preliminary experiments.

Category	Field	\mathcal{E}_θ	\mathcal{D}_ϕ	\mathcal{E}^p	DiT ^{DH}
Architecture	Input dim.	$224 \times 224 \times 3$	$16 \times 16 \times 768$	$224 \times 224 \times 3$	$16 \times 16 \times 768$
	Output dim.	$16 \times 16 \times 768$	$256 \times 256 \times 3$	$16 \times 16 \times 768$	$16 \times 16 \times 768$
	Hidden dim.	768	128	768	[1152, 2048]
	Num. layers	12	–	12	[28, 2]
	MLP Ratio	4	–	4	4
	Dim. per head	64	–	64	[72, 128]
	Num. heads	12	–	12	[16, 16]
	Channel mult.	–	[1, 1, 2, 2, 4]	–	–
	Res. blocks	–	2	–	–
	Attn. resolutions	–	16	–	–
	Total Params (M)	86.58M	44.8 M	86.58M	839M
Optimization	Training iters	4×10^4	4×10^4	–	10^5
	Batch size	512	512	–	1024
	Optimizer	AdamW	AdamW	–	AdamW
	Peak LR	2×10^{-4}	1×10^{-4}	–	2×10^{-4}
	LR Scheduler	Cosine	Cosine	–	Linear
	Warmup	1 epoch	–	–	40 epochs
	(β_1, β_2)	(0.9, 0.95)	–	–	(0.9, 0.95)
Interpolants	α_t	–	–	–	$1 - t$
	σ_t	–	–	–	t
	Training objective	reconstruction	reconstruction	–	v-prediction
	Sampler	–	–	–	Euler (ODE)
	Sampling steps	–	–	–	50
	Guidance	–	–	–	w/o CFG

Table 8: Class-conditional generation on ImageNet-1K at 256^2 . We report generation metrics for the diffusion model trained on the corresponding latents, evaluated both without and with CFG. † indicates reproduced results. Best and second-best results are highlighted in bold and underlined, respectively.

Method	Tokenizer	#Params	Epochs	Generation w/o CFG				Generation w/ CFG			
				gFID↓	IS↑	Prec.↑	Rec.↑	gFID↓	IS↑	Prec.↑	Rec.↑
<i>Generation Models w/o RM</i>											
MaskGIT[3]	VQGAN[40]	227M	555	6.18	182.1	<u>0.80</u>	0.51	–	–	–	–
LlamaGen[32]	VQGAN[40]	3.1B	300	9.38	112.9	0.69	0.67	2.18	263.3	0.81	0.58
MaskDiT-XL[46]	SD-VAE[29]	675M	1600	5.69	177.9	0.74	0.60	2.28	276.6	0.80	0.61
DiT-XL[26]	SD-VAE[29]	675M	1400	9.62	121.5	0.67	0.67	2.27	278.2	0.83	0.57
SiT-XL[24]	SD-VAE[29]	675M	1400	8.61	131.7	0.68	0.67	2.06	270.3	<u>0.82</u>	0.59
<i>External-RM Aligned Generation Models</i>											
REPA-XL [41]	SD-VAE[29]	675M	800	5.90	–	–	–	1.42	<u>305.7</u>	0.80	<u>0.65</u>
LightningDiT[39]	VA-VAE[39]	675M	800	2.17	205.6	0.77	<u>0.65</u>	1.35	295.3	0.79	<u>0.65</u>
<i>Internal-RM Generation Models</i>											
SVG-XL[30]	SVG[30]	675M	500	3.94	169.3	–	–	2.10	258.7	–	–
LightningDiT[39]	RAE-B[45]	676M	800	1.87	209.7	<u>0.80</u>	0.63	1.41	309.4	0.80	0.63
DiT ^{DH} -XL[45]	RAE-B [45]	839M	800	<u>1.51</u>	<u>242.9</u>	0.79	0.63	<u>1.13</u>	262.6	0.78	<u>0.67</u>
LightningDiT[39]	FAE-d32[11]	675M	800	1.48	239.8	0.81	0.63	1.29	268.0	0.80	0.64
LightningDiT[39]	RPiAE (Ours)	675M	800	1.68	254.7	0.79	0.63	1.09	272.1	0.75	0.70

C More Qualitative Results

We present more qualitative results in this section to further illustrate the performance of RPiAE across reconstruction, generation, and editing tasks.

C.1 Visualization of Image Reconstruction

Figure 6 shows qualitative results on the image reconstruction task. Compared with RAE, our method achieves clearly better reconstruction quality, especially in terms of structural accuracy and color fidelity. This advantage is particularly pronounced for regular geometric patterns, such as the wall tiles, mesh grids, fences, and honeycomb structures in the figure. Our reconstructions preserve these structures with clearer and more coherent textures, whereas RAE often fails to recover the correct structural details. In addition, our method produces more faithful colors, while RAE is prone to visible color deviations, such as overly saturated appearance in the rooster example and a greenish cast on the white wall.

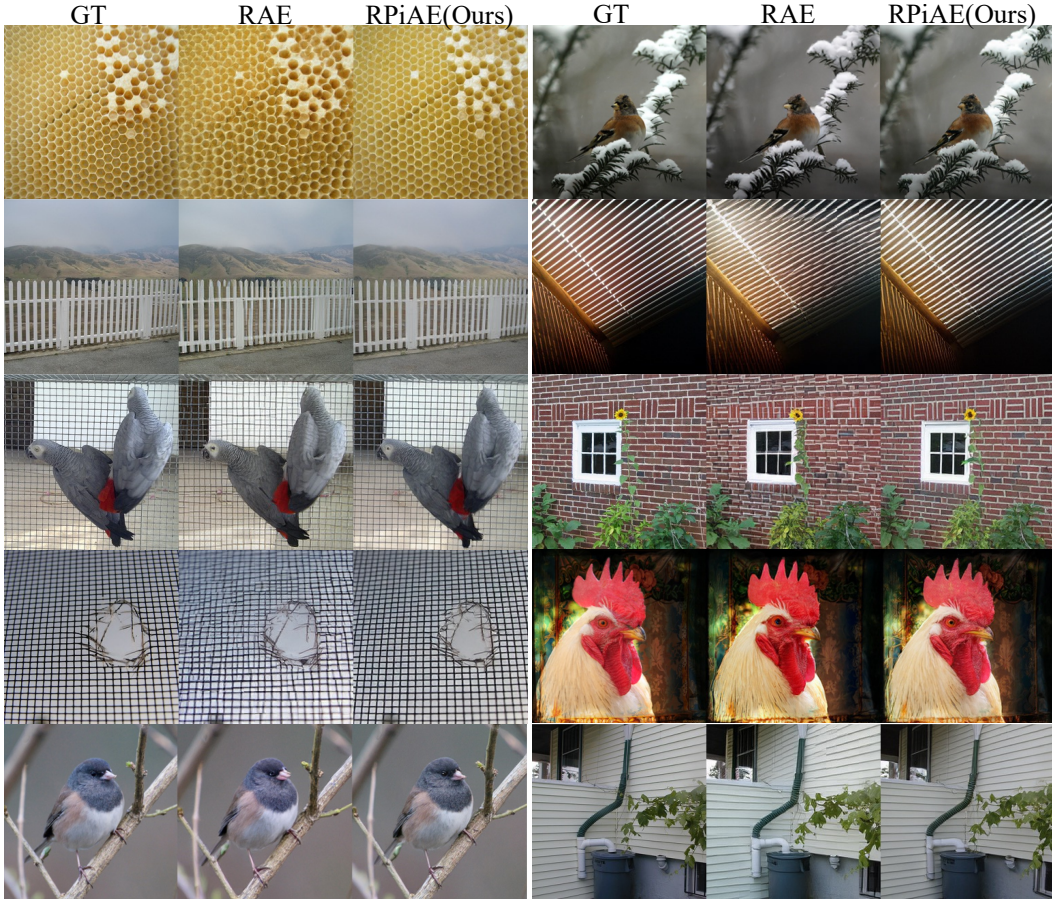


Figure 6: Qualitative comparison of image reconstruction results between our method and RAE. Our method achieves better reconstruction quality, particularly in preserving regular structural patterns and color fidelity. As shown in the examples, it reconstructs clearer and more plausible textures for structured regions such as wall tiles, mesh grids, fences, and honeycomb, while also reducing the color shifts that are visible in RAE reconstructions.

C.2 Visualization of Class-conditional Image Generation

Figure 7 presents selected class-conditional generation results on ImageNet-1K. The samples generated by our model are visually detailed and structurally plausible, with clear object boundaries, faithful part arrangements, and coherent overall composition. These results suggest that our method can support high-quality image synthesis while preserving fine-grained visual details.



Figure 7: Selected samples for class-conditional generation on ImageNet-1K at 256^2 .

C.3 More Visualization of Text-to-Image Generation

Figure 8 shows qualitative results on GenEval. Our method generates images with improved visual quality, exhibiting richer local details and more accurate object structures. In addition, the overall layouts are more coherent and better match the intended compositional relationships, indicating stronger generative performance on complex prompt-driven synthesis.

C.4 More Visualization of Image Edit

Figure 9 presents qualitative comparisons on image editing. Compared with the baselines, RPiAE follows the editing instructions more faithfully, yielding modifications that better match the intended semantic changes. Meanwhile, it retains strong reconstruction quality, preserving the original structure, appearance, and image coherence to a large extent. This suggests that RPiAE is particularly effective for editing scenarios that require both precise instruction following and faithful content preservation.

D Image Understanding

To examine whether the encoder semantics are preserved after training, we directly attach the pretrained DINOv2 classification head to the encoder learned by RPiAE and evaluate on ImageNet linear classification. Table 9 shows that the classification accuracy remains almost unchanged, with Top-1 accuracy dropping only from 84.56 to 84.18 and Top-5 accuracy from 97.04 to 96.91. This result suggests that Pivot Regularization effectively stabilizes the encoder during reconstruction training, allowing it to adapt to reconstruction while largely retaining the semantic structure inherited from the pretrained representation model.

Table 9: ImageNet linear probing results.

Model	Top-1 Acc. \uparrow	Top-5 Acc. \uparrow
DINOv2-B	84.56	97.04
RPiAE	84.18	96.91



Figure 8: More qualitative comparison on GenEval. Our method generates images with higher visual fidelity, richer details, and more accurate structural composition.

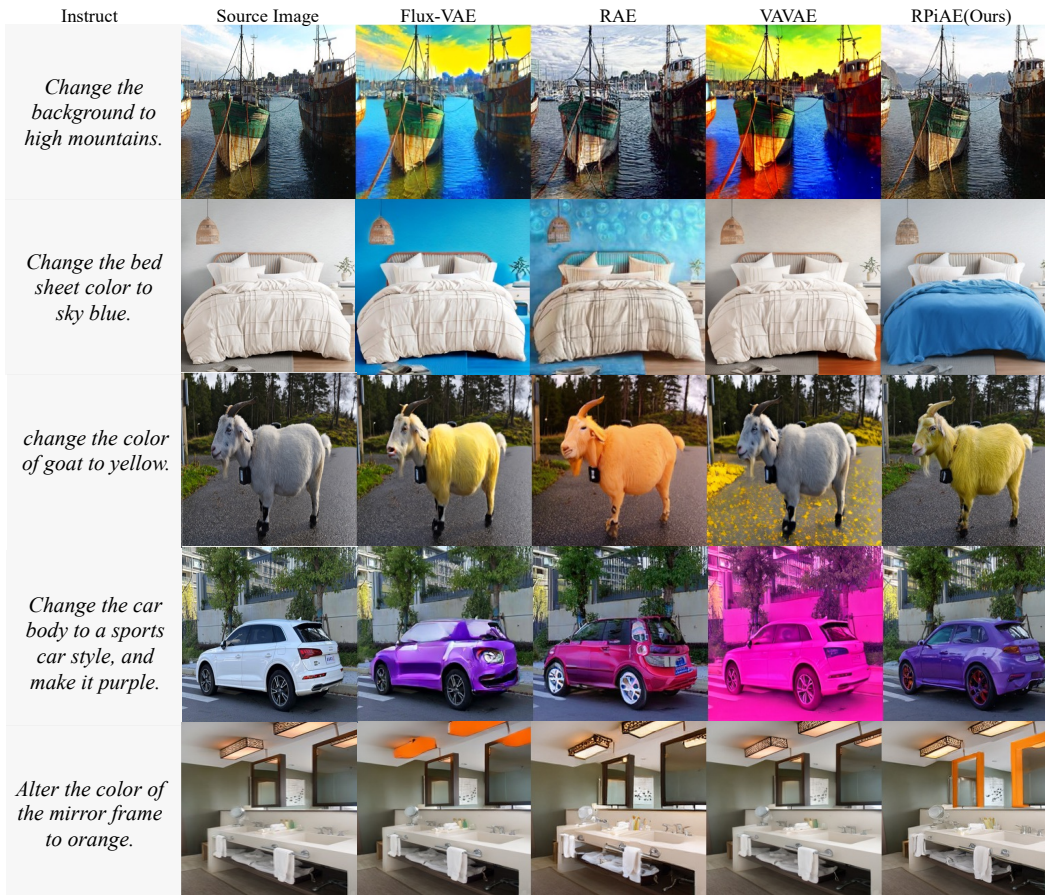


Figure 9: More qualitative comparison on image editing. RPiAE achieves the strongest instruction-following ability while maintaining high reconstruction quality.